

Every Nearby Energetic Pulsar Is Surrounded by a Region of Inhibited Diffusion

Isabelle John^{1,2,*} and Tim Linden^{3,4,†}

¹*Dipartimento di Fisica, Università degli Studi di Torino, via P. Giuria, 1 10125 Torino, Italy*

²*INFN – Istituto Nazionale di Fisica Nucleare, Sezione di Torino, via P. Giuria 1, 10125 Torino, Italy*

³*Stockholm University and The Oskar Klein Centre for Cosmoparticle Physics, Alba Nova, 10691 Stockholm, Sweden*

⁴*Erlangen Centre for Astroparticle Physics (ECAP), Friedrich-Alexander-Universität Erlangen-Nürnberg, Nikolaus-Fiebiger-Str. 2, 91058 Erlangen, Germany*

The H.E.S.S. telescope has recently detected the total electron-plus-positron (e^+e^-) flux up to 40 TeV, finding it to be a featureless and steeply-falling power-law above 1 TeV. This result is in stark tension with standard one-zone models of pulsar e^+e^- injection and diffusion, which predict a hard-spectrum signal above ~ 10 TeV. We model the local pulsar population, and find 20 sources that would each *individually* overproduce the H.E.S.S. e^+e^- flux in a one-zone diffusion model. We conclude that *every* energetic pulsar younger than ~ 500 kyr must be surrounded by a region of inhibited diffusion (*e.g.*, a supernova remnant, pulsar wind nebula, or TeV halo) that prevents the transport of these e^+e^- to Earth. Because the high-electron density in these regions produces bright synchrotron and inverse-Compton emission, we conclude that all nearby pulsars are detectable as (potentially unassociated) radio, x-ray or γ -ray sources.

Observations by the High-Energy Stereoscopic System (H.E.S.S.) have recently extended our detection of the combined electron-plus-positron (hereafter, e^+e^-) flux up to an energy of 40 TeV. The e^+e^- flux has a sharp break at an energy of ~ 1 TeV, above which the emission is characterized by a smooth and rapidly falling power-law, with $dN/dE \propto E^{-4.5}$ [1].

This observation strongly constrains the production and propagation of e^+e^- pairs from pulsars, which have long been considered to provide the dominant contribution to the local positron flux measured by PAMELA [2] and AMS-02 [3, 4] between ~ 10 –300 GeV [5–12]. As shown in Figure 1, the e^+e^- spectrum from nearby pulsars in a standard one-zone model has two components. The first is the steep rise at low energies that corresponds to electrons with cooling timescales (t_c) longer than the pulsar age (t_{PSR}). This component has a cutoff produced by the cooling of very high-energy electrons to a critical energy where $t_c = t_{\text{PSR}}$. The second, high-energy, component stems from recently produced e^+e^- that propagate to Earth before cooling. The relative energy-flux of each feature depends on the pulsar age, spindown time, injection spectrum, and distance, but are roughly similar.

By normalizing the GeV flux from pulsars to AMS-02 data, we can predict the H.E.S.S. TeV e^+e^- flux. The soft spectrum of the H.E.S.S. data then strongly constrains some convolution of the TeV e^+e^- injection rate from pulsars or the propagation of these pairs to Earth. Such a constraint has previously been applied to argue that e^+e^- propagation must be inhibited near bright pulsars such as Vela and Geminga [13–20].

In this *letter* we significantly extend this result to prove that diffusion must be inhibited around *every* pulsar (seen or unseen) that is either powerful enough, or

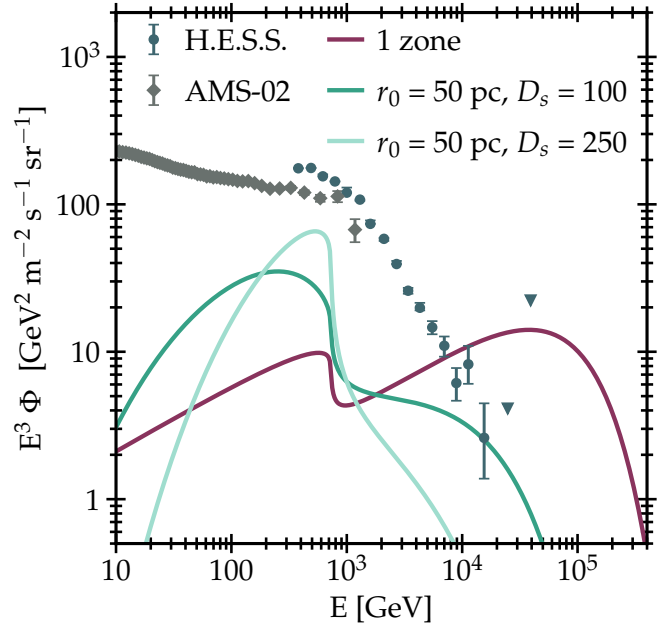


FIG. 1. The e^+e^- flux from a middle-aged pulsar (500 kyr old, 150 pc away) compared to H.E.S.S. (dark blue) [1] and AMS-02 (gray) [3, 4] data. The violet line corresponds to a one-zone diffusion model that overproduces the H.E.S.S. flux. Medium and light green represent two-zone diffusion models, where diffusion is inhibited around the pulsar. This suppresses the high-energy flux and agrees with data.

close enough, to contribute to the high-energy e^+e^- flux at Earth. Moreover, our analysis can be applied to any ensemble of pulsars that combine to contribute to the rising AMS-02 positron flux, regardless of their individual contributions. The argument proceeds as follows:

- (1) Recent observations of TeV halos [21–24] provide very strong evidence that pulsars produce the positron excess [9, 13, 25], establishing them as the predominant e^+e^- source near 1 TeV.

* Email: isabelle.john@unito.it; ORCID: [0000-0003-2550-7038](https://orcid.org/0000-0003-2550-7038)

† Email: linden@fysik.su.se; ORCID: [0000-0001-9888-0971](https://orcid.org/0000-0001-9888-0971)

- (2) Young pulsars produce most of their e^+e^- while rapidly spinning down soon after they are born [6]. However, the observation of bright TeV halos around Geminga and Monogem with γ -rays exceeding 50 TeV [26] establishes two key facts: (1) there is no a sharp cutoff in the pulsar e^+e^- injection at a few TeV, as e^+e^- up to ~ 100 TeV are needed to produce the γ -ray spectra, and (2) this e^+e^- acceleration must continue to late times, as these e^+e^- pairs cool in ~ 10 kyr. Recent HAWC, LHAASO, and H.E.S.S. measurements of TeV halos confirm that this phenomenon is generic, and not isolated to Geminga and Monogem [27–30].
- (3) In one-zone diffusion models, e^+e^- from sources within $\mathcal{O}(1)$ kpc of Earth can efficiently reach Earth before cooling, producing a bright ~ 10 TeV e^+e^- flux with a total power that is a few percent the peak pulsar power near the cutoff produced by e^+e^- cooling [19]. For many nearby pulsars, this e^+e^- flux will overproduce the H.E.S.S. data.
- (4) One method for decreasing the e^+e^- flux at Earth would be to produce a bubble of *locally* inhibited diffusion surrounding the solar position [22]. However, this provides a poor fit to the data for several reasons: (1) strongly inhibited diffusion near the Sun will prevent all e^+e^- from reaching the Earth, at odds with H.E.S.S. data [31], (2) a change in local diffusion will produce a common spectral cutoff that equally applies to all sources, producing a common spectral bump and fall-off (see Fig. 1) that does not fit the smooth power-law observed by H.E.S.S., (3) there are no known sources that could produce locally inhibited diffusion, while TeV halo observations indicate that many pulsars inhibit diffusion locally, (4) if locally inhibited regions of diffusion were common far from sources, it would significantly affect GeV secondary-to-primary ratios, significantly altering fits to AMS-02 data [9].

Based on these lines of evidence, there is only one remaining solution. Every pulsar that produces high-energy e^+e^- pairs must *also* produce a significant region of low-diffusion, which prevents these e^+e^- pairs from leaking into the interstellar medium (ISM) unperturbed. The origin of the inhibited diffusion is unclear, as both supernova remnants (SNR) and pulsar wind nebulae (PWNe) have long been assumed to inhibit diffusion in regions surrounding very young ($\lesssim 50$ kyr) pulsars [32–34]. However, by comparing current H.E.S.S. constraints against the ATNF pulsar catalog [35, 36], we can confirm that these inhibited diffusion regions continue to at least ~ 500 kyr, meaning that inhibited diffusion (most likely due to TeV halos) remains ubiquitous among middle-aged pulsars. Notably, these results are supported by γ -ray observations of middle-aged pulsars, which often show evidence of inhibited diffusion by factors of 100–1000 on scales of 25–50 pc [26].

The ubiquity of inhibited diffusion around pulsars allows us to make a second strong claim — all sufficiently nearby and energetic pulsars (very roughly within ~ 0.5 kpc for a 300 kyr pulsar) have either already been detected — or should very soon be detected as extended sources. The inhibition of diffusion means that any sufficiently nearby and young pulsar will produce bright TeV γ -ray emission independent of its beam orientation. The only caveats to this analysis are: (1) extremely dim pulsars whose TeV e^+e^- falls outside the normal pulsar population, (2) pulsars in regions of the sky that have not currently been covered by TeV instruments (primarily in the southern hemisphere), and (3) bright radio/TeV sources that are known, but not currently associated with pulsar activity.

Diffusion Models.— We calculate the e^+e^- flux from each individual pulsar using both one-zone and two-zone analytic diffusion models [5, 9, 19, 37]. Given a distance r from the pulsar to Earth and a pulsar age t_{PSR} , the e^+e^- flux is given by:

$$\Phi(E, r, t_{\text{PSR}}) = \frac{c}{4\pi} \int_0^{t_{\text{PSR}}} \frac{E_0^2}{E^2} Q(E_0, t') \mathcal{H}(r, E_0, t') dt', \quad (1)$$

where $Q(E_0, t')$ is the source term of injected e^+e^- normalized to the current spindown power of the pulsar, $\mathcal{H}(r, E_0, t')$ is a term describing diffusion, E (E_0) are the current (initial) energy of an e^\pm that was injected time $t = t_{\text{PSR}} - t'$ ago, which are related through $E_0 = E/(1 - Eb(E)t)$. The factor $b(E)$ denotes the energy losses of e^\pm during propagation, given by:

$$\frac{dE}{dt} = -b(E) E^2, \quad (2)$$

where b accounts for the magnetic field and interstellar radiation field that control the rate of synchrotron radiation and inverse-Compton scattering (see *e.g.* [9, 38]), respectively. We follow the analytic method in Ref. [38] with the ISRF model from Ref. [39]. We note that this analytic model neglects the stochastic nature of energy losses and approximates them as a continuous process; when the spectral shape of the pulsar is important (*e.g.* in searches for spectral features from pulsars in the e^+e^- data), this analytic model is insufficient, see Ref. [38]. However, this has negligible effects on our analysis, which gets its maximum constraining power well above the spectral feature produced by e^+e^- cooling.

The e^+e^- source term, $Q(E_0, t)$, is given by

$$Q(E_0, t) = \eta L(t) Q_0(E_0), \quad (3)$$

where η is the pulsar’s efficiency of converting its spindown luminosity $L(t)$ into e^+e^- pairs, with:

$$L(t) = L_0 \left(1 + \frac{t}{\tau}\right)^{-\frac{n+1}{n-1}}, \quad (4)$$

where L_0 is the initial pulsar luminosity, τ the spindown time scale, and $n = 3$ is the braking index for a dipole.

The e^+e^- injection spectrum $Q_0(E_0)$ is:

$$Q_0(E_0) = E_0^{-\alpha} \exp\left(-\frac{E_0}{E_{\text{cutoff}}}\right), \quad (5)$$

where α is the spectral index and E_{cutoff} is the cutoff energy for the e^+e^- accelerated by the pulsar. The integral over time in Eq. 1 accounts for the continuous injection of e^+e^- pairs by the pulsar.

In the *one-zone diffusion* model [5, 9], the diffusion factor \mathcal{H} becomes:

$$\mathcal{H} = \frac{1}{(4\pi\lambda^2(E_0, E))^{3/2}} \exp\left(-\frac{r^2}{4\lambda^2(E_0, E)}\right). \quad (6)$$

where the diffusion distance scale, λ , is given by:

$$\begin{aligned} \lambda^2(E_0, E) &= \int_E^{E_0} \frac{D(E')}{b(E')} dE' \\ &= \frac{D_1}{bE^{(1-\delta)}(1-\delta)} \left(1 - (1 - bEt)^{(1-\delta)}\right), \end{aligned} \quad (7)$$

and we set the diffusion coefficient $D(E)$ to be equal to an energy scaling of the diffusion constant D_1 , through:

$$D(E) = D_1 E^\delta. \quad (8)$$

In the *two-zone diffusion* model, diffusion is inhibited in a region r_0 around the pulsar, such that the diffusion constant D_0 in the inner zone is suppressed with respect to the standard interstellar diffusion constant D_1 , *i.e.*, $D_0 < D_1$, and \mathcal{H} becomes [19, 37]

$$\mathcal{H}(r, E, t) = \int_0^\infty \frac{\xi e^{-\psi}}{\pi^2 \lambda_0^2 r (A^2(\psi) + B^2(\psi))} \times \mathcal{D}(\psi) d\psi, \quad (9)$$

where the factor $\mathcal{D}(\psi)$ in the integrand for the one-zone diffusion model is

$$\mathcal{D}_{1\text{-zone}}(\psi) = \sin\left(\sqrt{\psi} \frac{r}{\lambda_0}\right) \quad (10)$$

and has the analytic solution given in Eq. 6. In the two-zone diffusion model, where $r \geq r_0$, this becomes

$$\begin{aligned} \mathcal{D}_{2\text{-zone}}(\psi) &= A(\psi) \sin\left(\sqrt{\psi} \frac{r\xi}{\lambda_0}\right) \\ &+ B(\psi) \cos\left(\sqrt{\psi} \frac{r\xi}{\lambda_0}\right). \end{aligned} \quad (11)$$

The factors A and B are defined as

$$\begin{aligned} A(\psi) &= \xi \cos(\chi) \cos(\xi\chi) + \sin(\chi) \sin(\xi\chi) \\ &+ \frac{1}{\chi} \left(\frac{1-\xi^2}{\xi} \sin(\chi) \cos(\xi\chi)\right) \end{aligned} \quad (12)$$

and

$$B(\psi) = \frac{\sin(\chi) - A(\psi) \sin(\xi\chi)}{\cos(\xi\chi)}, \quad (13)$$

where $\chi = \sqrt{\psi} \frac{r_0}{\lambda_0}$ and $\xi = \sqrt{\frac{D_0}{D_1}}$. Note that for one-zone diffusion, $A = 1$, $B = 0$ and $\xi = 1$. The diffusion distance in each zone is expressed in terms of λ_0 , which is related to D_0 , *i.e.* the suppressed diffusion constant, in Eq. 7.

For standard diffusion in the interstellar medium, we choose $D_{\text{ISM}} = 2 \times 10^{28} \text{ cm}^2/\text{s}$ at an e^+e^- energy of 1 GeV with a diffusion index of $\delta = 0.4$ [40, 41]. For two-zone diffusion, we set the size of the inner diffusion zone to $r_0 = 50 \text{ pc}$ and test a suppression factor $D_s = D_1/D_0$. We consider two cases, where $D_s = 100$ and 250, while $D_1 = D_{\text{ISM}}$. Note that the size of the diffusion zone r_0 and the suppression factor D_s are degenerate (when energy losses are neglected) via:

$$\ell = \sqrt{6Dt}, \quad (14)$$

where ℓ is the average distance an e^+e^- travels in a time t given a diffusion coefficient D (see Eq. 8) when energy losses are negligible. The time that the e^+e^- spend around the pulsar determines how much the high-energy portion of the flux is suppressed.

Pulsar Model.— We use the ATNF pulsar catalogue (version 2.6.0) that includes all known pulsars [35, 36], and select every pulsar with age and distance estimates indicating it is closer than 1.5 kpc and younger than 1 Myr. For our simulations, we use a generic pulsar model that we employ throughout our analysis. While in reality, each pulsar is expected to have different parameters that govern e^+e^- injection and diffusion (such as initial spindown luminosity, braking index, injection spectrum), our results are consistent across a wide-variety of ATNF pulsars, and thus changes in single systems do not significantly affect our results. We loosely base our generic pulsar model on Geminga [9], which stands as the best-measured middle-aged pulsar. For the pulsar injection spectrum, we use Eq. 5 with $\alpha = 2.0$ and $E_{\text{cutoff}} = 100 \text{ TeV}$. In Eq. 4, we set the initial spindown luminosity to $L(t=0) = 10^{38} \text{ erg/s}$ [21] and use a spindown timescale of $\tau = 10 \text{ kyr}$ [22], with a default e^+e^- efficiency of $\eta = 0.1$. We evaluate the contribution from our model pulsar system on a grid of ages that spans 5 kyr–1 Myr with a step size of 5 kyr and distances that span 100–1500 pc with a step size of 50 pc. We compare these gridded results to our population of ATNF systems.

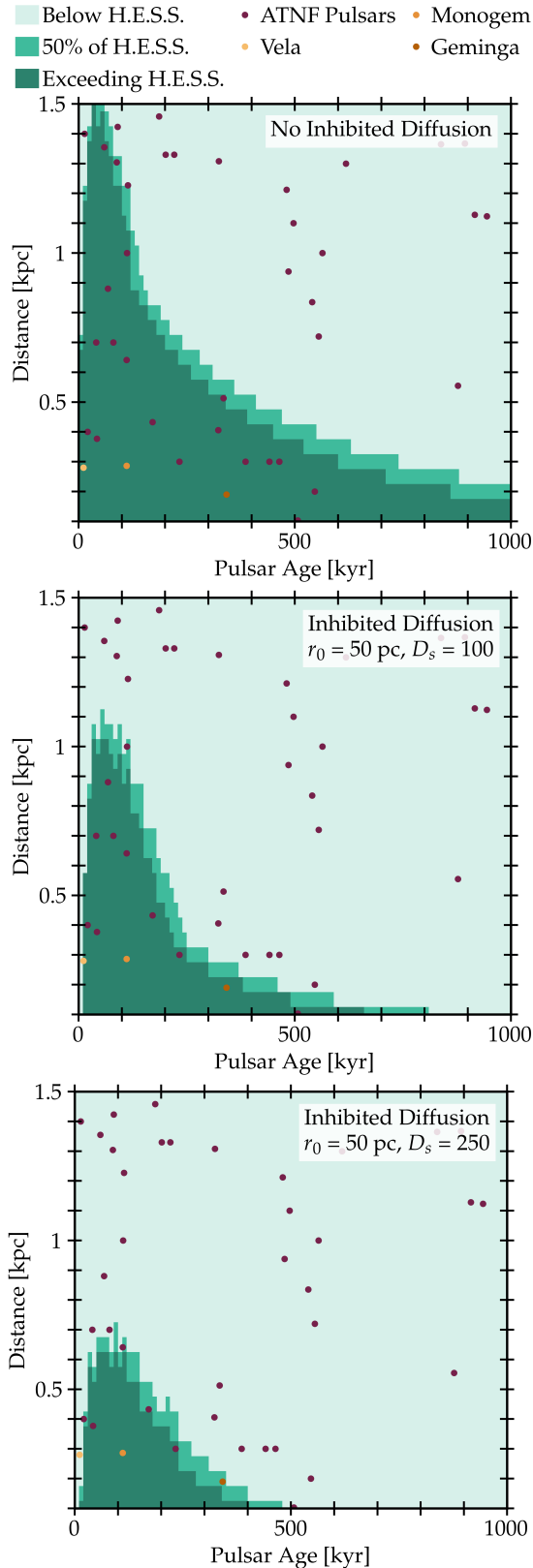


FIG. 2. The population of known pulsars that *individually* overproduce the H.E.S.S. e^+e^- data (dark green), account for 50% of H.E.S.S. (medium green), and less (light green), for the one-zone diffusion model (top panel), two-zone model for $r_0 = 50$ pc with $D_s = 100$ (middle panel) and $D_s = 250$ (bottom panel). Dots correspond to known ATNF pulsars.

Results and Discussion.— In Fig. 1, we compare the H.E.S.S. e^+e^- flux (dark blue) [1] with the e^+e^- spectrum of our generic pulsar model at an age of 500 kyr and distance of 150 pc. The standard one-zone model (violet) has a high-energy flux that significantly exceeds the H.E.S.S. data. In comparison, the dark (light) green spectrum represents a two-zone diffusion model where diffusion is suppressed by a factor of 100 (250) in a 50 pc region around the pulsar. These models produce TeV e^+e^- fluxes consistent with the data.

Figure 2 compares pulsars of different ages and distances to the H.E.S.S. e^+e^- data for our three diffusion models: the one-zone model (top panel), the two-zone model with $r_0 = 50$ pc and $D_s = 100$ (middle) and $r_0 = 50$ pc and $D_s = 250$ (bottom). Violet dots represent pulsars in the ATNF catalogue [35, 36], while Vela, Monogem and Geminga are shown with yellow, orange and dark orange dots, respectively. Pulsars in dark green regions have e^+e^- fluxes that would *individually* overproduce the H.E.S.S. data. Medium green regions represent pulsars which individually account for more than 50% of the flux in a single H.E.S.S. energy bin. Light green regions correspond to pulsars whose spectra fall below the H.E.S.S. data. In the one-zone model, ~ 20 known pulsars overproduce the H.E.S.S. data. The number reduces to 11 in the two-zone model with a $D_s = 100$ suppression, while in the case of $D_s = 250$ only three sources exceed the H.E.S.S. flux. We note that even this model does not saturate the potential for diffusion to be severely restricted near pulsars, as many pulsar wind nebulae as well as TeV halos like Geminga show evidence for diffusion to be inhibited by a factor of 1000 or more [26, 42].

Figure 3 shows the same result as Fig. 2 for models where we change the pulsar efficiency from $\eta = 10\%$ to 5% or 1%. This reduces the flux from each pulsar and reduces the number that exceed H.E.S.S. data. However, we find that for a 5% (1%) efficiency, 14 (5) pulsars still exceed H.E.S.S. data. Even for pulsars with much lower efficiencies than our standard scenario, inhibited diffusion is needed to be consistent with H.E.S.S.

Figure 4 shows how strongly diffusion must be suppressed for each of the 20 ATNF pulsars that overproduce the H.E.S.S. data in one-zone models. In this figure, we use the exact ages and distances for each pulsar. We note that the degree to which diffusion is suppressed and the size of the inhibited diffusion zone are degenerate. Thus, we fix the suppression factor to $D_s = 100$ and vary the size of the diffusion zone until the pulsar no longer overproduces H.E.S.S. data. The radius of inhibited diffusion can be smaller if diffusion is more strongly suppressed. In the top axis, we use Eq. 14 to approximate the time that a 10 TeV e^+e^- spends in the inhibited diffusion region. For comparison, if diffusion is not inhibited, a 10 TeV e^+e^- traverses 50 pc in only ~ 1600 yr.

Fig. 4 shows that e^+e^- must be trapped for more than 20 kyr in many systems, though the exact timescale varies. For example, 10-TeV e^+e^- from Monogem (J0559+1414) must be confined in a low diffusion re-

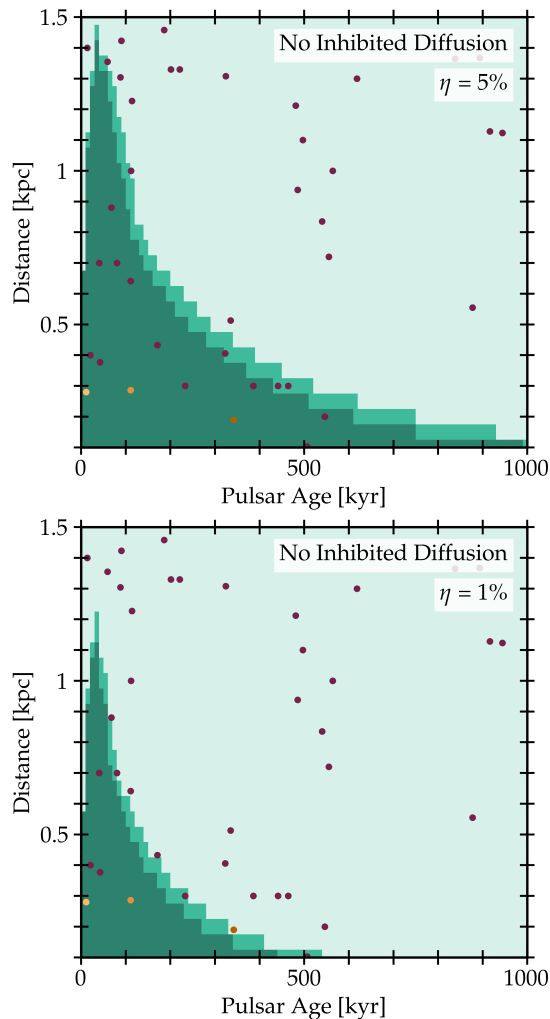


FIG. 3. Similar to Fig. 2 but for pulsar efficiencies of $\eta = 5\%$ (top) and $\eta = 1\%$ (bottom) instead of 10%.

gion for at least ~ 75 kyr, while e^+e^- from Geminga (J0633+1746) must only be confined for at least ~ 20 kyr.

We stress that, throughout this analysis, we only compare each pulsar individually to the H.E.S.S. data, while ignoring contributions from other pulsars. This means that our results are extremely conservative. Within the context of a one-zone model, the combined e^+e^- flux from all ATNF pulsars in our study would overproduce the H.E.S.S. e^+e^- flux unless the average efficiency of the pulsars was less than 0.1%, which falls far short of the known e^+e^- efficiency of multiple PWN and TeV halos. Even this constraint is conservative, as it omits known contributions from mis-aligned pulsars [21] and high-energy electrons accelerated in supernova remnants [43, 44].

Detection of Misaligned Pulsars — Numerous studies have investigated the potential for a mis-aligned pulsar to be discovered fortuitously close to Earth [45, 46]. In Ref. [21], we showed that TeV halo observations pro-

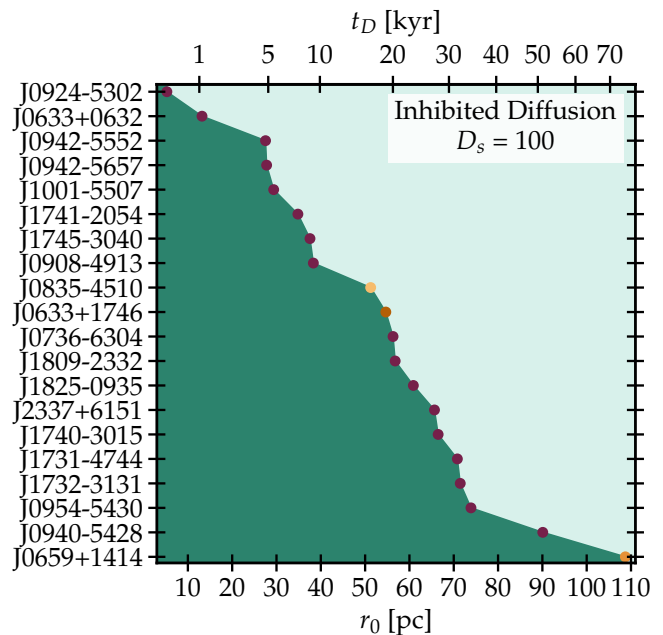


FIG. 4. The size of the inner diffusion zone, r_0 , which is needed for each ATNF pulsar to not overproduce the H.E.S.S. data. Diffusion is suppressed by a fixed value of $D_s = 100$. For smaller values of r_0 (dark green), the pulsar would overproduce H.E.S.S. data, while light green does not violate the data. The dots correspond to the critical r_0 . Vela, Monogem and Geminga are represented by yellow, orange and dark orange dots, respectively. Top axis shows the diffusion time scale, t_D , *i.e.*, the time that 10 TeV e^+e^- spend in the inhibited diffusion zone, estimated from Eq. 14 with $r_0 \approx \ell$.

vide a new potential method for detecting these pulsars. However, the detection of TeV halos around multiple sources did not *require* that all pulsars be surrounded by the necessary regions of inhibited diffusion (see also Ref. [13]). Here, we have shown that e^+e^- must be trapped for a significant duration around every energetic pulsar, which in turn requires that every energetic pulsar powers a bright PWN or TeV halo system.

In the supplemental material, we list the 20 nearby pulsars that overproduce the H.E.S.S. data within a one-zone diffusion model. We note that spatially extended emission has already been detected surrounding 12 of these systems, including every system in the northern hemisphere, which is better-covered at TeV energies. Our models indicate that the upcoming addition of CTA north and south [47, 48], as well as the proposed SWGO detector [49, 50], can potentially detect *all* remaining nearby pulsars, either providing new sources for novel probes of pulsar evolution and fundamental physics, or closing the possibility that such sources exist.

Summary and Outlook. — In this *letter*, we show that H.E.S.S. e^+e^- observations demand that a zone of inhibited diffusion must exist around every pulsar that is powerful and close enough to Earth. While observations

of both PWN and TeV halos around pulsars clearly show that pulsars are able to accelerate e^+e^- to hundreds of TeV, the steep fall of the e^+e^- flux above 1 TeV measured by H.E.S.S. rules out the strong e^+e^- contributions at tens of TeV as suggested by one-zone diffusion models. Instead, these observations require a zone of inhibited diffusion around pulsars which allows the e^+e^- to lose energy in the vicinity of the pulsar before reaching Earth. Our results further show that any pulsar powerful enough to produce high-energy e^+e^- must be a bright source, either in radio, x-ray or γ -rays, which has either already been detected, or soon will be detected by telescopes such as HAWC and LHAASO, as well as upcoming instruments such as CTA and SWGO.

Acknowledgements.— Many thanks to Benedikt Schroer for enlightening discussions on the two-zone diffusion model. IJ acknowledges support from the Research grant TAsP (Theoretical Astroparticle Physics) funded by INFN, and Research grant “Addressing systematic uncertainties in searches for dark matter”, Grant No. 2022F2843L funded by the Italian Ministry of University and Research (MUR). TL is supported by the Swedish Research Council under contract 2022-04283 and the Swedish National Space Agency under contract 117/19. TL also acknowledges sabbatical support from the Wenner- Gren foundation under contract SSh2024-0037.

Every Nearby Energetic Pulsar Is Surrounded by a Region of Inhibited Diffusion

Supplemental Material

Isabelle John, Tim Linden

I. SELECTED ATNF PULSARS

In our analysis, we include every pulsar found in the ATNF pulsar catalog [35, 36] that is within 1.5 kpc of Earth and less than 1 Myr old. In Table S1, we list the 20 pulsars that individually overproduce the H.E.S.S. e^+e^- in a one-zone diffusion model (Fig. 2, top panel), together with observations of an inhibited diffusion zone, which can be a supernova remnant (SNR), pulsar wind nebula (PWN) or TeV halo.

Pulsar	Age [kyr]	Distance [pc]	Inhibited Diffusion Zone
J0633+0632	59.2	1355	PWN [51]
J0633+1746	342	190	TeV halo [22]
J0659+1414	111	286	TeV halo [22]
J0736-6304	507	103	TeV halo candidate [45] ^a
J0835-4510	11.3	280	TeV halo [27]
J0908-4913	112	1000	SNR, PWN [52]
J0924-5302	335	513	–
J0940-5428	42.2	377	–
J0942-5552	464	300	–
J0942-5657	323	406	–
J0954-5430	171	433	PWN candidate [53]
J1001-5507	441	300	–
J1731-4744	80.4	700	–
J1732-3131	111	641	–
J1740-3015	20.6	400	PWN, TeV halo [54]
J1741-2054	386	300	PWN [55, 56]
J1745-3040	546	200	SNR candidate [57]
J1809-2332	67.6	880	SNR, PWN [58]
J1825-0935	233	300	–
J2337+6151	40.6	700	SNR [59]

^a Ref. [45] finds hints for an extended γ -ray emission around J0736-6304 in the context of a different analysis.

TABLE S1. The ages and distances of the 20 pulsars which individually overproduce the H.E.S.S. e^+e^- flux in our one-zone diffusion model for an e^+e^- injection efficiency of 10%. We list potential sources for the inhibition of diffusion (SNR, PWN, TeV Halos), but note that multiple physical effects could be present that combine to inhibit the efficiency of diffusion. [60, 61].

II. REDUCED e^+e^- EFFICIENCY

In our standard scenario in the main text, we assume an efficiency of converting spindown power into e^+e^- pairs of $\eta = 10\%$, based on estimates of Geminga [9]. However, if Geminga is unusually bright, a lower efficiency might be favoured for other pulsars. We therefore also compare our pulsar models to the H.E.S.S. data assuming efficiencies of 5% and 1%. Fig. 3 show both scenarios in the one-zone diffusion model. Figure S1 shows the pulsar population for the two choices of the two-zone diffusion model, as in Fig. 2 for the 5% and 1% efficiencies, respectively. As can be seen, even for a significantly lower pulsar efficiency, that results in a lower flux, the one-zone diffusion model overproduces the data for 14 and 5 sources in the 5% and 1% scenario, respectively, requiring a zone of inhibited diffusion.

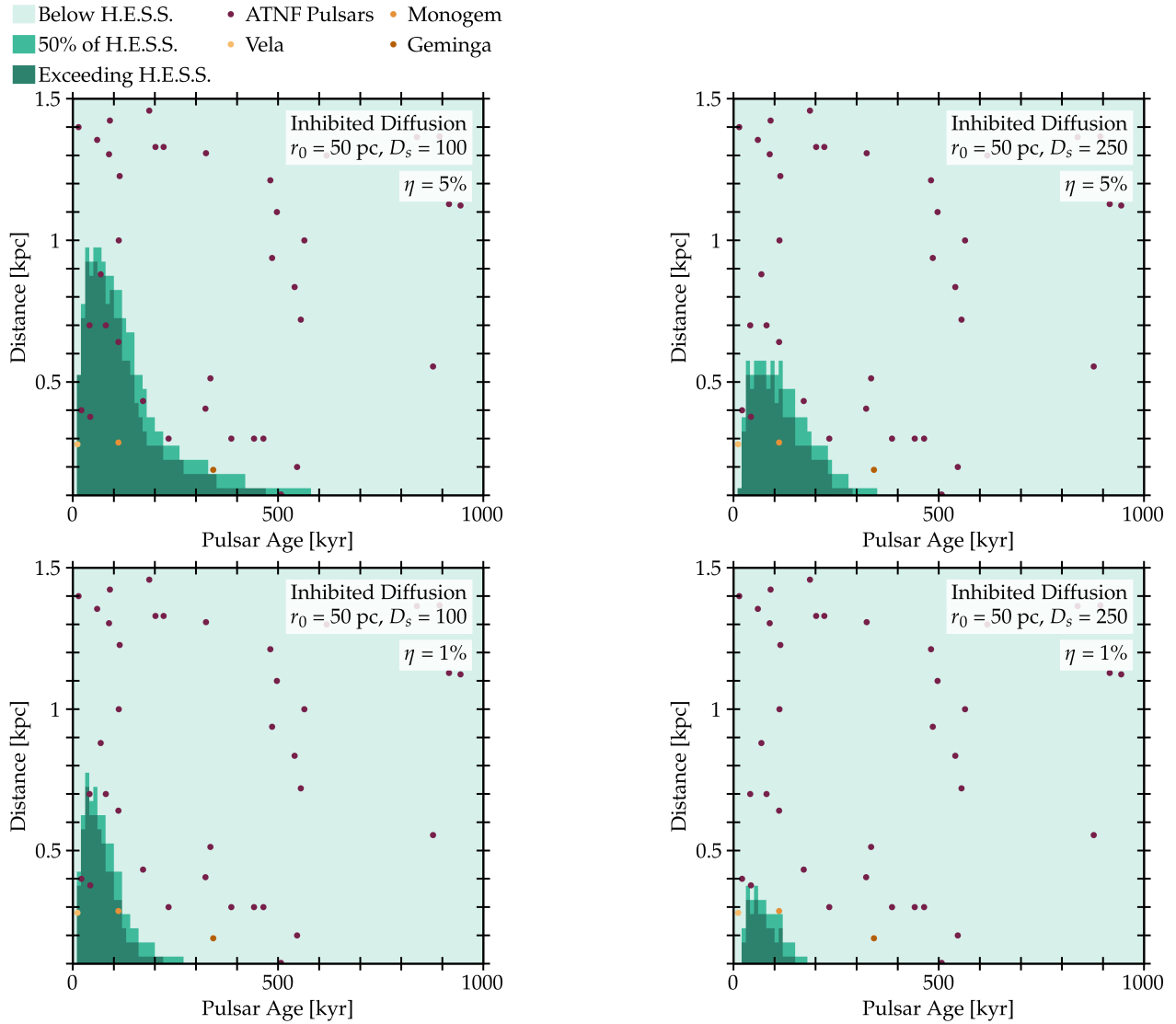


FIG. S1. Same as Fig. 2 but with a pulsar efficiency of $\eta = 5\%$ (top panels) and $\eta = 1\%$ (bottom panels) for the two-zone diffusion model.

III. PROJECTION TO FUTURE TELESCOPES

Upcoming telescopes such as the Cherenkov Telescope Array (CTA) [47, 48] are expected to measure the e^+e^- flux even further to energies of hundreds of TeV. This will allow us to further constrain the e^+e^- flux from pulsars that dominantly contribute at energies of hundreds of TeV.

We project the potential constraints based on future CTA observations of the high-energy e^+e^- flux by extrapolating the H.E.S.S. data to \sim PeV by following the powerlaw provided by [1] that describes the flux for energies above the 1-TeV break with a spectral index of $\Gamma = 4.49$.

We show our results in Figure S2, which is similar to Fig. 2, except that the light blue regions represent pulsars that exceed the e^+e^- in the extrapolated energy range. We find that CTA will be able to significantly constrain a much larger population of relatively old pulsars, though, at present there are no known pulsars which inhibit the age- and distance- range probed by CTA observations.

[1] F. Aharonian *et al.* (H.E.S.S.), *Phys. Rev. Lett.* **133**, 221001 (2024), arXiv:2411.08189 [astro-ph.HE].

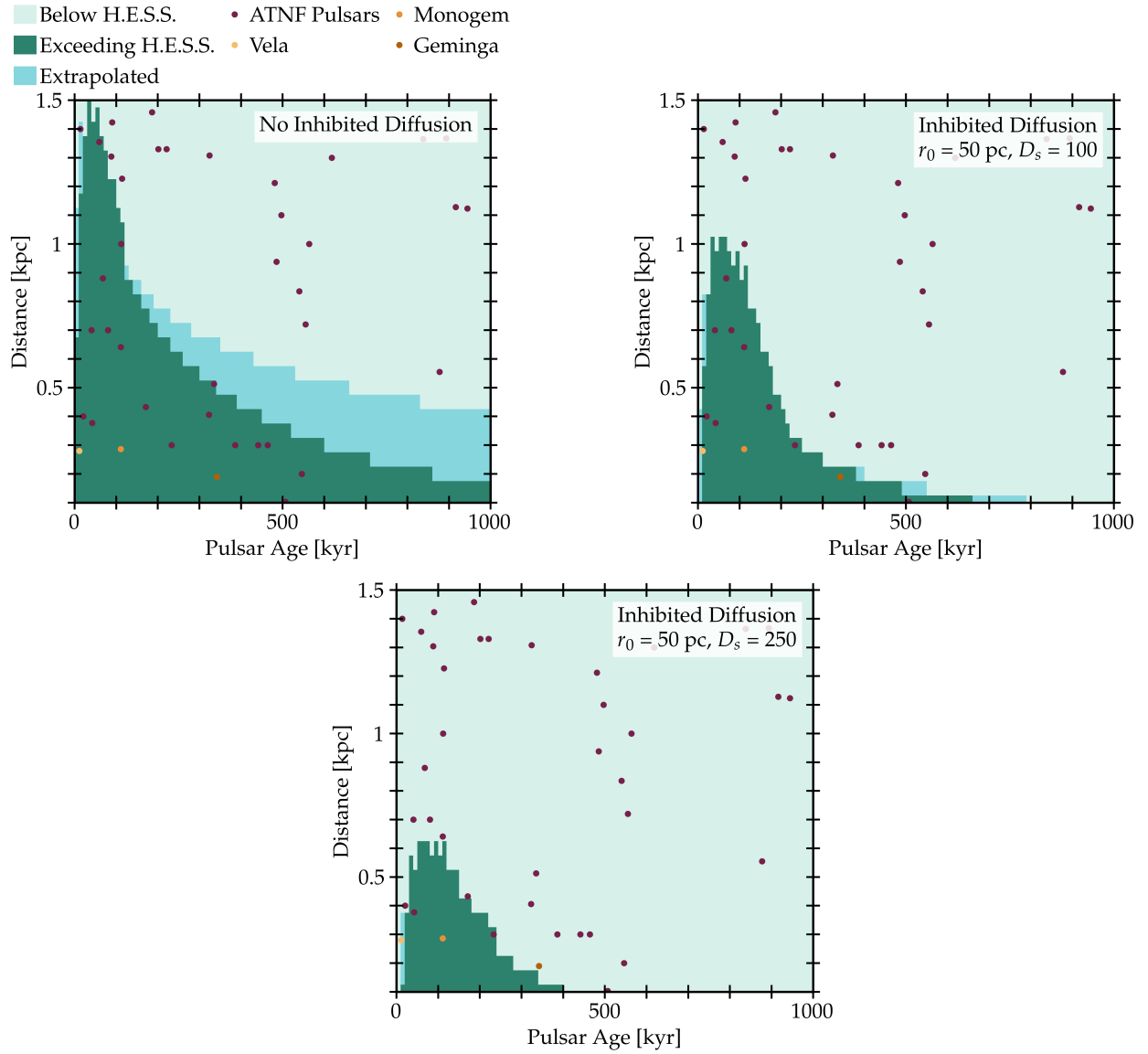


FIG. S2. Same as Fig. 2, but including a projection of the H.E.S.S. data following a powerlaw with $\Gamma = 4.49$ [1], that extends the exclusion of pulsars that would exceed the H.E.S.S. data at energies above the H.E.S.S. range, represented by light blue regions.

- [2] O. Adriani *et al.* (PAMELA), *Phys. Rev. Lett.* **111**, 081102 (2013), arXiv:1308.0133 [astro-ph.HE].
- [3] M. Aguilar, L. Ali Cavazonza, G. Ambrosi, and et al. (AMS Collaboration), *Phys. Rev. Lett.* **122**, 041102 (2019).
- [4] M. Aguilar, L. Ali Cavazonza, B. Alpat, and et al. (AMS Collaboration), *Phys. Rev. Lett.* **122**, 101101 (2019).
- [5] D. Hooper, P. Blasi, and P. D. Serpico, *JCAP* **01**, 025 (2009), arXiv:0810.1527 [astro-ph].
- [6] S. Profumo, *Central Eur. J. Phys.* **10**, 1 (2011), arXiv:0812.4457 [astro-ph].
- [7] D. Malyshev, I. Cholis, and J. Gelfand, *Phys. Rev. D* **80**, 063005 (2009), arXiv:0903.1310 [astro-ph.HE].
- [8] T. Linden and S. Profumo, *Astrophys. J.* **772**, 18 (2013), arXiv:1304.1791 [astro-ph.HE].
- [9] D. Hooper, I. Cholis, T. Linden, and K. Fang, *Phys. Rev. D* **96**, 103013 (2017), arXiv:1702.08436 [astro-ph.HE].
- [10] L. Orusa, S. Manconi, F. Donato, and M. Di Mauro, *JCAP* **12**, 014 (2021), arXiv:2107.06300 [astro-ph.HE].
- [11] I. Cholis and I. Krommydas, *Phys. Rev. D* **105**, 023015 (2022), arXiv:2111.05864 [astro-ph.HE].
- [12] L. Orusa, S. Manconi, F. Donato, and M. Di Mauro, *JCAP* **02**, 029 (2025), arXiv:2410.10951 [astro-ph.HE].
- [13] S. Profumo, J. Reynoso-Cordova, N. Kaaz, and M. Silverman, *Phys. Rev. D* **97**, 123008 (2018), arXiv:1803.09731 [astro-ph.HE].
- [14] Z.-Q. Huang, K. Fang, R.-Y. Liu, and X.-Y. Wang, *Astrophys. J.* **866**, 143 (2018), arXiv:1807.04182 [astro-ph.HE].
- [15] X. Tang and T. Piran, *Mon. Not. Roy. Astron. Soc.* **484**, 3491 (2019), arXiv:1808.02445 [astro-ph.HE].
- [16] C. Evoli, T. Linden, and G. Morlino, *Phys. Rev. D* **98**, 063017 (2018), arXiv:1807.09263 [astro-ph.HE].

- [17] M. Di Mauro, S. Manconi, and F. Donato, *Phys. Rev. D* **100**, 123015 (2019), [Erratum: *Phys.Rev.D* 104, 089903 (2021)], [arXiv:1903.05647 \[astro-ph.HE\]](#).
- [18] S. Manconi, M. Di Mauro, and F. Donato, *Phys. Rev. D* **102**, 023015 (2020), [arXiv:2001.09985 \[astro-ph.HE\]](#).
- [19] B. Schroer, C. Evoli, and P. Blasi, *Phys. Rev. D* **107**, 123020 (2023), [arXiv:2305.08019 \[astro-ph.HE\]](#).
- [20] K. Fang, *Phys. Rev. D* **109**, 043041 (2024), [arXiv:2310.16594 \[astro-ph.HE\]](#).
- [21] T. Linden, K. Auchettl, J. Bramante, I. Cholis, K. Fang, D. Hooper, T. Karwal, and S. W. Li, *Phys. Rev. D* **96**, 103016 (2017), [arXiv:1703.09704 \[astro-ph.HE\]](#).
- [22] A. U. Abeysekara *et al.* (HAWC), *Science* **358**, 911 (2017), [arXiv:1711.06223 \[astro-ph.HE\]](#).
- [23] F. Aharonian *et al.* (H.E.S.S.), *Astron. Astrophys.* **673**, A148 (2023), [arXiv:2304.02631 \[astro-ph.HE\]](#).
- [24] Z. Cao *et al.* (LHAASO), *Astrophys. J. Suppl.* **271**, 25 (2024), [arXiv:2305.17030 \[astro-ph.HE\]](#).
- [25] K. Fang, X.-J. Bi, P.-F. Yin, and Q. Yuan, *Astrophys. J.* **863**, 30 (2018), [arXiv:1803.02640 \[astro-ph.HE\]](#).
- [26] A. Albert, R. Alfaro, C. Alvarez, J. C. Arteaga-Velázquez, D. Avila Rojas, H. A. Ayala Solares, R. Babu, E. Belmont-Moreno, A. Bernal, K. S. Caballero-Mora, T. Capistrán, A. Carramiñana, S. Casanova, U. Cotti, J. Cotzomi, S. Coutiño de León, E. de la Fuente, D. Depaoli, N. Di Lalla, R. Diaz Hernandez, B. L. Dingus, M. A. DuVernois, M. Durocher, J. C. Díaz-Vélez, K. Engel, C. Espinoza, K. L. Fan, K. Fang, N. Fraija, J. A. García-González, F. Garfias, H. Goksu, M. M. González, J. A. Goodman, S. Groetsch, J. P. Harding, S. Hernández-Cadena, I. Herzog, P. Hüntemeyer, D. Huang, F. Hueyotl-Zahuantitla, A. Iriarte, V. Joshi, S. Kaufmann, D. Kieda, A. Lara, W. H. Lee, J. Lee, H. León Vargas, J. T. Linnemann, A. L. Longinotti, G. Luis-Raya, K. Malone, O. Martinez, J. Martínez-Castro, J. A. Matthews, P. Miranda-Romagnoli, J. A. Montes, J. A. Morales-Soto, E. Moreno, M. Mostafá, A. Nayerhoda, L. Nellen, R. Noriega-Papaqui, L. Olivera-Nieto, N. Omodei, Y. Pérez Araujo, E. G. Pérez-Pérez, C. D. Rho, D. Rosa-González, H. Salazar, D. Salazar-Gallegos, A. Sandoval, M. Schneider, G. Schwefer, J. Serna-Franco, Y. Son, R. W. Springer, O. Tibolla, K. Tollefson, I. Torres, R. Torres-Escobedo, R. Turner, F. Urea-Mena, E. Varela, L. Villaseñor, X. Wang, I. J. Watson, E. Willox, H. Wu, S. Yun-Cárcamo, H. Zhou, C. de León, and M. Di Mauro, *ApJ* **974**, 246 (2024).
- [27] T. Sudoh, T. Linden, and J. F. Beacom, *Phys. Rev. D* **100**, 043016 (2019), [arXiv:1902.08203 \[astro-ph.HE\]](#).
- [28] F. Aharonian *et al.* (LHAASO), *Phys. Rev. Lett.* **126**, 241103 (2021), [arXiv:2106.09396 \[astro-ph.HE\]](#).
- [29] A. Albert *et al.* (HAWC), *Astrophys. J. Lett.* **911**, L27 (2021), [arXiv:2101.07895 \[astro-ph.HE\]](#).
- [30] F. Aharonian *et al.* (H.E.S.S.), *Astron. Astrophys.* **672**, A103 (2023), [arXiv:2302.13663 \[astro-ph.HE\]](#).
- [31] D. Hooper and T. Linden, *Phys. Rev. D* **98**, 083009 (2018), [arXiv:1711.07482 \[astro-ph.HE\]](#).
- [32] J. Vink, *A&A Rev.* **20**, 49 (2012), [arXiv:1112.0576 \[astro-ph.HE\]](#).
- [33] B. M. Gaensler and P. O. Slane, *Ann. Rev. Astron. Astrophys.* **44**, 17 (2006), [arXiv:astro-ph/0601081](#).
- [34] A. M. W. Mitchell and J. Gelfand, (2022), [10.1007/978-981-16-4544-0_157-1](#), [arXiv:2208.11026 \[astro-ph.HE\]](#).
- [35] R. N. Manchester, G. B. Hobbs, A. Teoh, and M. Hobbs, *Astron. J.* **129**, 1993 (2005), [arXiv:astro-ph/0412641](#).
- [36] “ATNF Pulsar Catalogue Website,” <http://www.atnf.csiro.au/research/pulsar/psrcat>.
- [37] S. M. Osipov, A. M. Bykov, A. E. Petrov, and V. I. Romansky, *J. Phys. Conf. Ser.* **1697**, 012009 (2020).
- [38] I. John and T. Linden, *Phys. Rev. D* **107**, 103021 (2023), [arXiv:2206.04699 \[astro-ph.HE\]](#).
- [39] T. A. Porter, I. V. Moskalenko, A. W. Strong, E. Orlando, and L. Bouchet, *Astrophys. J.* **682**, 400 (2008), [arXiv:0804.1774 \[astro-ph\]](#).
- [40] M. Korsmeier and A. Cuoco, *Phys. Rev. D* **105**, 103033 (2022), [arXiv:2112.08381 \[astro-ph.HE\]](#).
- [41] M. Di Mauro, M. Korsmeier, and A. Cuoco, *Phys. Rev. D* **109**, 123003 (2024), [arXiv:2311.17150 \[astro-ph.HE\]](#).
- [42] M. Di Mauro, S. Manconi, and F. Donato, *Phys. Rev. D* **101**, 103035 (2020), [arXiv:1908.03216 \[astro-ph.HE\]](#).
- [43] T. Kobayashi, Y. Komori, K. Yoshida, and J. Nishimura, *Astrophys. J.* **601**, 340 (2004), [arXiv:astro-ph/0308470](#).
- [44] G. Morlino and S. Celli, *Mon. Not. Roy. Astron. Soc.* **508**, 6142 (2021), [arXiv:2106.06488 \[astro-ph.HE\]](#).
- [45] S. J. Lloyd, P. M. Chadwick, and A. M. Brown, *Phys. Rev. D* **100**, 063005 (2019), [arXiv:1908.03413 \[astro-ph.HE\]](#).
- [46] M. Baryakhtar, J. Bramante, S. W. Li, T. Linden, and N. Raj, *Phys. Rev. Lett.* **119**, 131801 (2017), [arXiv:1704.01577 \[hep-ph\]](#).
- [47] “<https://www.cta-observatory.org>.”
- [48] J. Knödlseider (CTA Consortium), in *16th Rencontres du Vietnam: Theory meeting experiment: Particle Astrophysics and Cosmology* (2020) [arXiv:2004.09213 \[astro-ph.IM\]](#).
- [49] “<https://www.swgo.org/swgowiki/doku.php>.”
- [50] H. Schoorlemmer (SWG0), *PoS ICRC2019*, 785 (2020), [arXiv:1908.08858 \[astro-ph.HE\]](#).
- [51] A. Danilenko, A. Karpova, D. Ofengeim, Y. Shibanov, and D. Zyuzin, *Mon. Not. Roy. Astron. Soc.* **493**, 1874 (2020), [arXiv:2001.10968 \[astro-ph.HE\]](#).
- [52] S. Johnston and M. E. Lower, *Mon. Not. Roy. Astron. Soc.* **507**, L41 (2021), [arXiv:2108.09827 \[astro-ph.HE\]](#).
- [53] Y.-C. Ding, N. Li, C.-C. Wei, Y.-L. Wu, and Y.-F. Zhou, *Phys. Rev. D* **103**, 115010 (2021), [arXiv:2007.00703 \[astro-ph.HE\]](#).
- [54] O. Kargaltsev and G. G. Pavlov, in *X-ray Astronomy 2009; Present Status, Multi-Wavelength Approach and Future Perspectives*, American Institute of Physics Conference Series, Vol. 1248, edited by A. Comastri, L. Angelini, and M. Cappi (AIP, 2010) pp. 25–28, [arXiv:1002.0885 \[astro-ph.HE\]](#).
- [55] F. Camilo, P. S. Ray, S. M. Ransom, M. Burgay, T. J. Johnson, M. Kerr, E. V. Gotthelf, J. P. Halpern, J. Reynolds, R. W. Romani, P. Demorest, S. Johnston, W. van Straten, P. M. Saz Parkinson, M. Ziegler, M. Dormody, D. J. Thompson, D. A. Smith, A. K. Harding, A. A. Abdo, F. Crawford, P. C. C. Freire, M. Keith, M. Kramer, M. S. E. Roberts, P. Weltevrede, and K. S. Wood, *ApJ* **705**, 1 (2009), [arXiv:0908.2626 \[astro-ph.GA\]](#).
- [56] M. Marelli, A. Belfiore, P. Saz Parkinson, P. Caraveo, A. De Luca, C. Sarazin, D. Salvetti, G. R. Sivakoff, and F. Camilo, *Astrophys. J.* **790**, 51 (2014), [arXiv:1404.1532 \[astro-ph.HE\]](#).
- [57] F. Aharonian (H.E.S.S.), *Astron. Astrophys.* **483**, 509 (2008), [arXiv:0803.2844 \[astro-ph\]](#).

- [58] A. Van Etten, R. W. Romani, and C.-Y. Ng, *The Astrophysical Journal* **755**, 151 (2012).
- [59] E. Furst, W. Reich, and J. H. Seiradakis, *A&A* **276**, 470 (1993).
- [60] P. Mukhopadhyay and T. Linden, *Phys. Rev. D* **105**, 123008 (2022), arXiv:2111.01143 [astro-ph.HE].
- [61] K. Fang, X.-J. Bi, and P.-F. Yin, *Mon. Not. Roy. Astron. Soc.* **488**, 4074 (2019), arXiv:1903.06421 [astro-ph.HE].